Hindawi
Wireless Communications and Mobile Computing
Volume 2022, Article ID 8991316, 14 pages
https://doi.org/10.1155/2022/8991316

Research Article

A Training Sequence-Based Ranging Method for R-Mode of VHF Data Exchange System

Xiaowen Sun, Qing Hu, and Yi Jiang

College of Information Science and Technology, Dalian Maritime University, Linghai Road No. 1, Dalian 116026, China

Correspondence should be addressed to Xiaowen Sun; sunxiaowen_1984@163.com

Received 15 February 2022; Revised 22 March 2022; Accepted 6 April 2022; Published 5 May 2022

Academic Editor: Mu Zhou

Copyright © 2022 Xiaowen Sun et al. This is an open access article distributed under the Creative Commons Attribution License, which permits unrestricted use, distribution, and reproduction in any medium, provided the original work is properly cited.

The space-time reference provided by GNSS is the basis of the 6G mobile communication integrating land, sea, air, and space. But GNSS has natural vulnerability. In order to solve this problem at sea, ships should be equipped with both space-based and land-based positioning and navigation systems in the future. The Ranging Mode (R-Mode) of the existing maritime communication system is an economical land-based backup positioning system, which is also an important support for e-Navigation. This paper proposes a pseudorange measurement method based on training sequence with multicorrelators, which can be used in the R-Mode of the VHF data exchange system (VDES). This method uses the correlation property of the ASM and VDE training sequence in the VDES for ranging. It reproduces the training sequence in the receiver, and then, noncoherent correlates with the received signal, meanwhile using the pseudorange measurement method with multicorrelators to reduce the influence of pulse shaping on the correlation curve. This paper also gives a design of receiver to implement the proposed method. Experiments are carried out based on the receiver to evaluate the ranging performance. The results show that, compared with the traditional maximum correlation value and E-L methods, the multicorrelator method can effectively reduce the ranging error. When E_s/N_0 is greater than 15 dB, the ranging accuracy of the proposed method can be better than 3 m. With the proposed method, the VDES signal can be used for both ranging and communication. Compared with the general VDES function, it does not occupy any additional time slot resources. This provides a reference for the future research of the VDES R-Mode, which can be used to solve the vulnerability problem of the GNSS on maritime communication.

1. Introduction

The global internet of things in the land, sea, air, and space, that is, the 6G mobile communication system, will deeply integrate navigation, communication, and remote sensing technologies [1–3]. And the space-time reference provided by GNSS is an important basis for the integration. However, the GNSS is vulnerable to unintentional or intentional interference, which leads to the loss or error of Position, Navigation, and Timing (PNT) information due to the weakness of the signals. The International Maritime Organization (IMO) has been considering the vulnerability of GNSS for a long time and suggests the development of land-based radio navigation systems as an effective and reliable solution to this problem [4, 5]. World Wide Radio Navigation Plan (WWRNP) pointed out that the ships should be equipped with both space-based and land-based positioning and navigation systems in the future to ensure its safety [6]. The R-Mode land-based positioning and navigation system uses electronic measurement to get the distance between the ship and the base station for positioning. It can make full use of the existing shore-based equipment, saving the infrastructure construction costs.

Automatic Identification System (AIS) is a widely used maritime communication system for exchanging relevant information between ships and base stations operating in the very high-frequency (VHF) radio band around 162 MHz [7]. The member states of IMO have been leading in and enforcing the use of AIS in the analysis of ship-to-ship collisions, vessel monitoring, and maritime traffic management offshore [8]. AIS also plays an important role

in avoiding ship collisions and protecting ship safety. However, with the increase of the number of ships, AIS channel overload has become an urgent problem for some ports [9]. In 2012, the International Telecommunication Union (ITU) first proposed the concept of VHF data exchange system (VDES) [10]. It is an enhanced and upgraded system of AIS in the VHF radio band 156.025–162.025 MHz. Based on the existing AIS channel, it adds the special application message (ASM) channel and broadband very high-frequency data exchange (VDE) channel, which can effectively relieve the slot pressure of data exchange in AIS. VDES also adds the function of satellite communication; that is, the VDE channel includes VDE-Terrestrial (VDE-TER) and VDE-Satellite (VDE-SAT), and the ASM channel includes ASM-TER and ASM-SAT [11, 12]. The VDES provides a variety of means for the exchange of data between maritime stations, ship-to-ship, ship-to-shore, shore-to-ship, ship-to-satellite, and satellite-to-ship. It provides an effective auxiliary mean for the safety of ship and comprehensively improves the capability and frequency efficiency of marine data communication [13]. The VDES has been established as an important component of future maritime communication systems in e-Navigation by IMO [14, 15].

The VDES is a communication system, and its R-Mode uses communication signals for ranging and positioning. The signals originally designed for communication also carry pseudorange measurement information, which can be used for ranging. Such signals are signals of opportunity (SOP). In recent years, more and more scholars began to research on the navigation via signal of opportunity (NAVSOP). NAVSOP regards all potential radio signals in the surrounding environment as SOP and extracts location and time information for navigation from them [16]. In the urban and indoor environment where GNSS signals are seriously blocked, the surrounding SOP can be used to assist the positioning. It can greatly improve the positioning accuracy without adding any sensors or transmitters [17–19]. The mobile signals can be SOP for each other in mobile wireless positioning [20–22]. The GNSS signals can combine with the SOP such as WCDMA (Wideband Code Division Multiple Access), LTE (Long-Term Evolution), UWB (Ultra Wideband), and broadcast signals to enhance the GNSS positioning [23–26]. The SOP can also be integrated into the integrated navigation of Inertial Navigation System (INS) and GNSS. It can assist GNSS positioning in complex environment [27–29]. The existence, availability, and combination are the unique attributes of the SOP, which are both advantages and challenges.

Although there are many NAVSOP-related researches on land, there are relatively much less such researches in maritime field. The European Union-funded Accessibility for Shipping, Efficiency Advantages and Sustainability (ACCSEAS) project demonstrated the feasibility of R-Mode using MF DGPS, AIS, and e-Loran transmissions [30–32], and reference [33] extended the theoretical analysis of ranging precision to the VDES R-Mode. The Chinese AIS ship Autonomous Positioning System (AAPS) project realized the positioning function of AIS R-Mode system [34, 35] and carried out the theoretical research of the VDES R-Mode [36]. Based on that, the AIS/VDES R-Mode testbed was built in the Yellow Sea and Bohai Sea in China. Meanwhile, R-Mode Baltic project built the R-Mode testbed in the Baltic Sea and researched on both MF and VHF R-Mode [37–39]. In the studies of R-Mode pseudorange measurement method in the VDES, reference [40] used GMSK modulated AIS communication signal for ranging, which had low accuracy. And reference [41] used the special pseudorandom sequence of VDE channel for ranging, which can get higher accuracy. But it needed specific time slots for the sequence transmission and occupied the communication time slots for the ranging. In the latest researches on VDES R-Mode, reference [42] considered the system security and proposed the concept of authentication, and reference [43] investigated the feasibility of a satellite-based component to VDES R-Mode. These studies are also based on the special pseudorandom sequence of VDE channel.

This paper proposes a pseudorange measurement method of multicorrelators based on training sequence for the VDES R-Mode. It can realize high-accuracy ranging while communicating, without occupying any additional time slot resources. It uses the correlation property of the training sequence of ASM-TER (terrestrial) and VDE-TER communication message in the VDES for ranging. $\pi/4$ QPSK modulation is used for the training sequence that is composed of Barker13 and inverted Barker13 codes with good correlation property. The receiver reproduces the IF signal of training sequence, and noncoherent correlates it with the received signal. And it uses multicorrelator pseudorange measurement method to reduce the influence of pulse shaping on the correlation curve to improve the ranging accuracy.

The main contributions of this paper include the following: (1) we propose a ranging method based on the VDES training sequence, which is normally used to capture and synchronize the communication signal. It can provide a reference for the future research of the VDES R-Mode; (2) we discuss the influence of the pulse shaping in the VDES on the ranging performance. This is a new scientific problem for R-Mode of communication system like VDES; (3) we give a receiver design with a structure of multicorrelator, which can be used to realize the ranging method proposed in this paper. It can reduce the influence of the pulse shaping on the ranging performance and realize high-accurate ranging function without occupying any additional time slot resources.

The proposed method in this paper can be used in VDES R-Mode receiver to measure the pseudorange between the receiver and the base station that transmit the communication signals. Since the location of the base station is known, the receiver can calculate its position by solving the pseudorange equations when it gets the pseudoranges of more than three base stations.

The rest of the paper is organized as follows: Section 2 introduces the theoretical principle of the ranging method based on the training sequence in the VDES; Section 3 introduces the implementation of the training sequence-based multicorrelator ranging method; Section 4 shows the simulation results and analysis of the ranging performance; and Section 5 summarizes the main conclusions.

2. Theoretical Principle of the VDES Ranging Method

2.1. Ranging Signal in the VDES

2.1.1. Terrestrial Subsystems of the VDES. The VDES includes three subsystems: AIS, ASM, and VDE. This paper only deals with the terrestrial component of the VDES, because the current satellite component is not suitable for positioning for their location cannot be accurately provided to the users all the time [33]. The technical specifications of the VDES terrestrial component are summarized in Table 1.

The AIS uses two 25 kHz channels (AIS 1 and AIS 2) for ship position reporting and other safety-related applications. It uses Gaussian Minimum Shift Keying (GMSK) modulation. The symbol rate, $R_S = 1/T_S$, is 9600 symbols/s (sps), where each symbol has one bit, that is, 9600 bits/s (bps).

The ASM-TER uses two 25 kHz channels (ASM 1 and ASM 2) and $\pi/4$ Quaternary Phase Shift Keying ($\pi/4$ QPSK) modulation. It gives a high reliability of message delivery and message acknowledgement support. The symbol rate, R_S is 9600 sps, where each symbol has two bits, that is, 19200 bps.

The VDE-TER has 100 kHz bandwidth which can optionally be configured to work as 50 kHz or 25 kHz bandwidth. It can also be configured to use $\pi/4$ QPSK, Eight-state Phase Shift Keying (8-PSK), or 16-state Quadrature Amplitude Modulation (16-QAM) modulations [44]. The symbol rate R_S increases from 19200 sps to 76800 sps with the increase of bandwidth. The bit rate depends not only on symbol rate but also on the modulation mode.

2.1.2. $\pi/4$ QPSK Modulation. The proposed method in this paper is based on the $\pi/4$ QPSK modulated training sequence in ASM channel and VDE channel.

The $\pi/4$ QPSK is a modulation technique which is developed in QPSK and offset QPSK (OQPSK) and is often used in differential coding [45, 46]. It has twice the bandwidth efficiency of the BPSK, since two bits are transmitted in a single modulation symbol. The kth symbol of the $\pi/4$ QPSK modulated baseband signal s_k in the interval of $kT_s \le t \le (k+1)T_s$ can be expressed as

$$s_k = \sqrt{2\frac{E_s}{T_s}}e^{j\theta_k}, \tag{1}$$

where T_s is the symbol interval, E_s is the energy per symbol, and θ_k is the phase of the kth symbol.

In $\pi/4$ QPSK, the maximum phase change is limited to $\pm 3\pi/4$, as compared to π for QPSK and $\pi/4$ for OQPSK. Therefore, the bandlimited $\pi/4$ QPSK signal preserves the constant envelope property better than bandlimited QPSK but is more susceptible to envelope variations than OQPSK [47].

A more attractive feature of $\pi/4$ QPSK is that it can be noncoherently detected, which greatly simplifies receiver design [47–50]. In this paper, we make use of this feature and implement the proposed method with a noncoherent receiver structure.

2.1.3. Signal Used for Ranging. A frame in the VDES equals one minute and is divided into 2250 slots; that is, each slot lasts about 26.67 milliseconds (ms). The general slot format of ASM-TER and VDE-TER is shown in Table 2. Each slot consists of six parts: ramp up, training sequence, link ID, data, ramp down, and guard. The ramp up time from −50 dBc to −1.5 dBc of the power is 416 microseconds (μs), to provide spectral shaping and reduce interference, and the modulation is not specified for the ramp up. The training sequence is the focus of this paper, which will be introduced in detail in the next paragraph. The link ID follows the training sequence and uses $\pi/4$ QPSK modulation to define the channel configurations. The data payload with its Cyclic Redundancy Check (CRC) is interleaved encoded scrambled and bit mapped. The ramp down time from full power to −50 dBc should be no more than 416 μs. The rest guard time is for delay and jitter.

The ranging method proposed in this paper is based on the training sequence of ASM-TER and VDE-TER. It is a 27-symbol training sequence and uses $\pi/4$ QPSK modulation. The last 26 symbols are Barker 13 code (1 1 1 1 1 0 0 1 1 0 1 0 1) and inverted Barker 13 code (0 0 0 0 0 1 1 0 0 1 0 1 0) with ideal autocorrelation, which can be used to detect the weak target signal submerged in noise. And this paper uses the ideal autocorrelation of the double Barker 13 code for ranging. In the training sequence, the symbol "1" maps to $\pi/4$ QPSK symbol "3" (1 1), and the symbol "0" maps to $\pi/4$ QPSK symbol "0" (0 0).

Figure 1 shows the bit mapping for $\pi/4$ QPSK used in ASM-TER and VDE-TER and the phase alternating of the training sequence. There are 4 possible phase variations of $\pm\pi/4$ and $\pm 3\pi/4$ when the symbol changes. Since there are only "11" and "00" in the training sequence, without "01" and "10," it has only four kinds of phase alternating as shown in Figure 1. The first the symbol "1" of the training sequence maps to $\pi/4$ QPSK symbol "3" (1 1) is mapped to the constellation defined by the point $(1+j)/\sqrt{2}$; the next symbol "1" is mapped to the constellation defined by point $1+0j$ (shown in blue in Figure 1); the next symbol "1" is mapped to the constellation defined by point $(-1-\mathrm{j})/\sqrt{2}$ (shown in green in Figure 1), and so on.

2.2. Theoretical Principle

2.2.1. Noncoherent Correlation of the Training Sequence. The 27 symbols of the training sequence can be serial-parallel inverted into in-phase (I) and quadrature (Q) branches with the same values; that is, the values of I and Q branches of the kth symbol are $s_{Ik} = s_{Qk} = 0$ or $s_{Ik} = s_{Qk} = 1$. After the bit mapping shown in Figure 1, the signals of I and Q branches can be expressed as follows:

$$I_k = \cos\theta_k = I_{k-1}\cos\phi_k - Q_{k-1}\sin\phi_k, \tag{2}$$

$$Q_k = \sin\theta_k = I_{k-1}\sin\phi_k - Q_{k-1}\cos\phi_k, \tag{3}$$

where

Table 1: The technical specifications of the VDES terrestrial component.

Subsystems	Signal bandwidth	Modulations	Symbol rate	Bit rate
AIS	25 kHz	GMSK	9.6 ksps	9.6 kbps
ASM-TER	25 kHz	$\pi/4$ QPSK	9.6 ksps	19.2 kbps
VDE-TER	25 kHz/ 50 kHz/ 100 kHz	$\pi/4$ QPSK/ 8-PSK/ 16-QAM	19.2 ksps (25 kHz)/ 38.4 ksps (50 kHz)/ 76.8 ksps (100 kHz)	Depends on the modulation and the symbol rate

Table 2: ASM-TER and VDE-TER general slot format.

Ramp up	Training sequence	Link ID	Data	Ramp down	Guard
0.41 ms	27 symbols (1 1111100110101 0000011001010)	16 symbols	Data with CRC	0.41 ms	0.83 ms

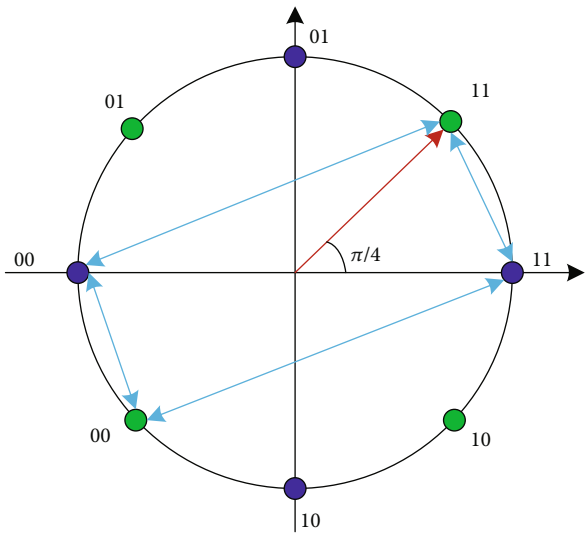

Figure 1: Bit mapping for $\pi/4$ QPSK and phase alternating of the training sequence.

$$\theta_k = \theta_{k-1} + \phi_k, \tag{4}$$

where θ_k and θ_{k-1} are the phases of the kth and the $k-1$st symbols and ϕ_k is the phase shift of the kth symbol compared with the $k-1$st symbol. The value of ϕ_k can be $\pm \pi/4$ and $\pm 3\pi/4$ depending on the input symbols. According to Figure 1, the value of ϕ_k can be determined by the kth symbol s_k, the $k-1$st symbol s_{k-1} and the initial values of s_k and θ_k. The specific values of these $\pi/4$ QPSK modulation parameters of the first 10 symbols in the training sequence are as shown in Table 3. The initial values of s_k and θ_k are $s_0 = 1$ and $\theta_0 = \pi/4$.

The baseband signals of the I and Q branches shown in equations (2) and (3) are, respectively, multiplied by the in-phase carrier signal $\cos \omega_c t$ and the quadrature carrier signal $-\sin \omega_c t$, and then, add the two branches signal to complete the carrier modulation. After that, within the kth symbol duration of $kT_s \le t \le (k+1)T_s$, the $\pi/4$ QPSK modulated signal can be expressed as

$$\begin{aligned} s_k(t) &= I_k \cos \omega_c t - Q_k \sin \omega_c t \\ &= \cos \theta_k \cos \omega_c t - \sin \theta_k \sin \omega_c t \\ &= \cos (\omega_c t + \theta_k), \end{aligned} \tag{5}$$

If the receiver can locally reproduce the modulated wave of $\pi/4$ QPSK, its frequency is the same as the received signal from the transmitter, and the phase is not necessarily the same; then, the locally reproduced signal can also be divided into I and Q branches. The signals of I and Q branches in the time interval of $kT_s \le t \le (k+1)T_s$ can be, respectively, expressed as

$$l_{Ik}(t) = I_k \cos (\omega_c t + \alpha) - Q_k \sin (\omega_c t + \alpha) = \cos (\omega_c t + \alpha + \theta_k), \tag{6}$$

$$l_{Qk}(t) = I_k \sin (\omega_c t + \alpha) - Q_k \cos (\omega_c t + \alpha) = -\sin (\omega_c t + \alpha + \theta_k). \tag{7}$$

By multiplying the received signal from the transmitter as equation (5) and the I and Q signals reproduced by the receiver as equations (6) and (7), respectively, and then integrating them, the results are as follows:

$$ac_{Ik} = \int_{kT_s}^{(k=1)T_s} \cos (\omega_c t + \theta_k) \cos (\omega_c t + \alpha + \theta_k) dt = \frac{T_s}{2} \cos \alpha, \tag{8}$$

$$ac_{Qk} = -\int_{kT_s}^{(k=1)T_s} \cos (\omega_c t + \theta_k) \sin (\omega_c t + \alpha + \theta_k) dt = \frac{T_s}{2} \sin \alpha. \tag{9}$$

Equations (8) and (9) give the integration results of I and Q branches in a symbol time interval of $kT_s \le t \le (k+1)T_s$. If all the 26 symbols of the double Barker codes are integrated, the results are also determined by the autocorrelation of the double Barker codes. Meanwhile, in order to remove the influence of the carrier phase difference between the reproduced signal and the received signal, that is, α, the noncoherent correlation is carried out.

Table 3: $\pi/4$ QPSK modulation parameters in the training sequence.

k	θ_k	ϕ_k	s_k	s_{k-1}
0	$\pi/4$	/	1	/
1	0	$-\pi/4$	1	1
2	$\pi/4$	$\pi/4$	1	1
3	0	$-\pi/4$	1	1
4	$\pi/4$	$\pi/4$	1	1
5	0	$-\pi/4$	1	1
6	$-3\pi/4$	$-3\pi/4$	0	1
7	+/-π	$-\pi/4$	0	0
8	$\pi/4$	$-3\pi/4$	1	0
9	0	$-\pi/4$	1	1
10	$-3\pi/4$	$-3\pi/4$	0	1
…	…	…	…	…

The receiver reproduces the last 26 symbols of the training sequence, which are the double Barker codes. The I and Q branches are multiplied with the received signal from the transmitter and then integrated, respectively. The integral results of I and Q branches are then squared, respectively, and then, the two results are added to get the noncoherent correlation value as follows:

$$\mathrm{Cor} = \mathrm{CF} \cdot \left[\left(\sum_{k=0}^{N-1} ac_{Ik} \right)^2 + \left(\sum_{k=0}^{N-1} ac_{Qk} \right)^2 \right] = \mathrm{CF} \cdot N^2 \cdot \frac{T_s^2}{4}, \tag{10}$$

where $N = 26$ indicates the number of the integrated symbols and CF is the correlation factor, which can be expressed as follows:

$$\mathrm{CF} = \frac{1}{N} \cdot \sum_{i=0}^{N} [\mathrm{ms}(i) - \mathrm{ns}(i)], \tag{11}$$

where ms is the number of matched symbols and ns is the number of mismatched symbols. According to the structure of the training sequence shown in Table 2, if the first symbol of the link configuration ID is 0, as received sequence shown in Figure 2, CF is the maximum value of 1 when the local reproduced 26 symbols exactly match the received signal for ms which is 26 and ns which is 0. And CF is the minimum value of 0 when the locally reproduced 26 symbols are 1 symbol time Ts earlier or later than the received signal, for ms is 13 and ns is 13, as shown in Figure 2.

Assuming that the time deviation between the local reproduced signal and the received signal is $\Delta\tau$, when $-T_s \le \Delta\tau \le T_s$, CF can be expressed as

$$\mathrm{CF}(\Delta\tau) = 1 - \frac{|(\Delta\tau)|}{T_s}. \tag{12}$$

2.2.2. The TOA Ranging. Ranging system based on radio signal is essentially a measurement system of transmission delay [51], so is the VDES R-Mode. The transmitter sends out the radio signal at the start of the slot, expressed as t_T. When the local reproduced sequence in the receiver completely matches the sequence of the received signal, that is, $\Delta\tau$ is 0, the time of arrival (TOA) can be obtained. The difference between TOA and t_T is the transmission delay, expressed as Δt. The distance between the transmitter and the receiver is the result of multiplying the transmission delay Δt by the speed of the electromagnetic wave c, as shown in equation (13). This distance is also known as pseudorange, because the value of distance is not accurate due to the influence of the clock difference between the transmitter and the receiver.

$$d = c \cdot \Delta t = c \cdot (\mathrm{TOA} - t_T). \tag{13}$$

Thus, the time deviation between the local reproduced signal and the received signal $\Delta\tau$ can be determined by the correlation value. When the correlation value is maximum, $\Delta\tau$ is the ideal case of 0. The TOA can be determined by $\Delta\tau$. Since the transmission time t_T is fixed at the beginning of the slot, it is easy to get the pseudorange measurement value according to formula (12).

2.3. Influence of the Pulse Shaping. When rectangular pulses are passed through a bandlimited channel, the pulses will spread in time, and the pulse for each symbol will smear into the time intervals of succeeding symbols. This causes Intersymbol Interference (ISI) and leads to an increased probability of the receiver making an error in detecting a symbol [47]. To solve this problem, spectral shaping is usually done through baseband or IF processing, since it is difficult to directly manipulate the transmitter spectrum at RF frequencies. There are some pulse shaping techniques including Nyquist criterion [52], (root) raised cosine roll-off filter, and Gaussian pulse shaping filter which can be used to reduce the ISI and reduce the bandwidth of a modulated signal.

In order to improve the communication quality of VDES and reduce Intersymbol Interference (ISI), the baseband shall employ a root raised cosine filter with roll-off factor 0.35 in ASM channel and 0.30 in VDE channel for the pulse shaping:

$$H(f) = \begin{cases} 1 & 0 \le |f| \le \dfrac{1-\beta}{2T_s}, \\ \sqrt{\dfrac{1}{2}\left[1 + \cos\left(\dfrac{\pi(|f| \cdot 2T_s - 1 + \beta)}{2\beta}\right)\right]} & \dfrac{1-\beta}{2T_s} < |f| < \dfrac{1+\beta}{2T_s}, \\ 0 & |f| \ge \dfrac{1+\beta}{2T_s}, \end{cases} \tag{14}$$

where $\beta = 0.35$ in the ASM channel and $\beta = 0.30$ in the VDE channel.

After pulse shaping using equation (14), Figure 3(a) shows the correlation curves of in 4 different cases.

Received:	1	1	1	1	1	1	0	0	1	1	0	1	0	1	0	0	0	0	0	1	1	0	0	1	0	1	0	0	
Local 1 symbol Earlier:	1	1	1	1	1	0	0	1	1	0	1	0	1	0	0	0	0	0	1	1	0	0	1	0	1	0			ms = 13; ns = 13
Local Prompt:		1	1	1	1	1	0	0	1	1	0	1	0	1	0	0	0	0	0	1	1	0	0	1	0	1	0		ms = 26; ns = 0
Local 1 symbol Later:			1	1	1	1	1	0	0	1	1	0	1	0	1	0	0	0	0	0	1	1	0	0	1	0	1	0	ms = 13; ns = 13

Figure 2: Number of matched symbols (ms) and number of mismatched symbols (ns).

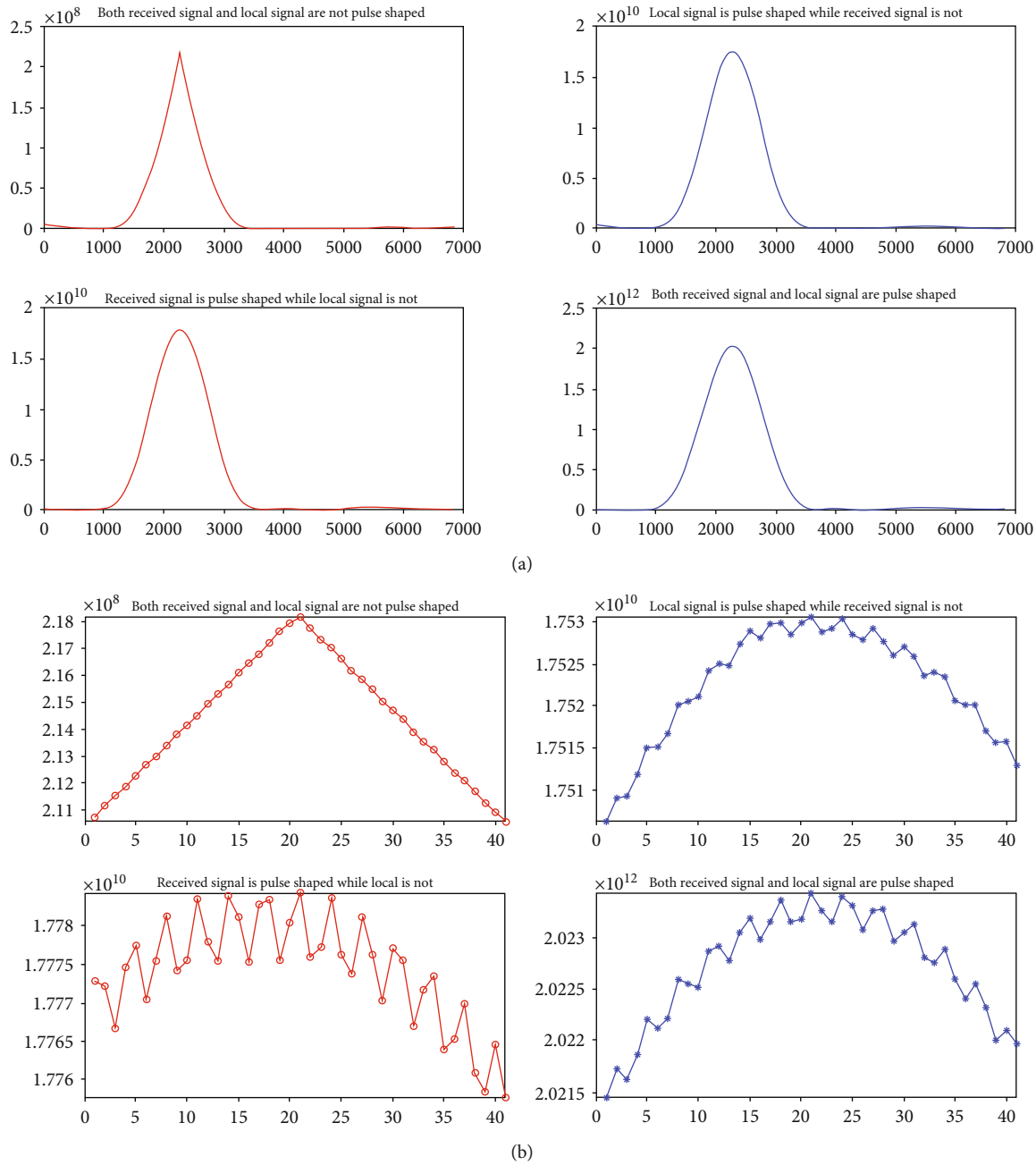

Figure 3: Correlation curves in 4 different cases: (a) the whole correlation curves; (b) the amplificated correlation curves with the maximum correlation value as the center.

Figure 3(b) shows the amplification result with the maximum correlation value as the center.

In the first case, when pulse shaping was not carried out for both the received signal and the local reproduced signal, the correlation value and $\Delta\tau$ are ideal linear relation that met equations (10), (11), and (12). It can be seen from the first figures in Figures 3(a) and 3(b) that the points of correlation values form a symmetrical triangle. The point of maximum value is the synchronous phase.

In the other three cases, when pulse shaping was carried out for the received signal or/and the local reproduced signal, the shape of the correlation curve changed, and the linear relation between the correlation value and $\Delta\tau$ was worse. It can be seen from the rest three figures in Figures 3(a) and 3(b) that the points of correlation values are not asymmetric. The point of maximum value is not the synchronous phase.

3. Implementation of the Proposed Method

3.1. Structure of Proposed VDES R-Mode Receiver. Take the ASM channel receiver as an example. The structure shown in Figure 4 can be used for communication and ranging at the same time. The signal received by the antenna first goes through the Radio Frequency (RF) front-end circuit; after downconversion, Analog-Digital (A/D) sampling, it then becomes the digital Intermediate Frequency (IF) signal, which is connected to the IF circuit. $\pi/4$ QPSK demodulation for ASM messages and correlation processing for TOA are carried out at the same time in the IF circuit. The processor uses the demodulated ASM message for normal data communication and uses the TOA measurement value for positioning.

In the RF circuit, the input signals are sampled by 120 MHz clock signal. The ASM 1 channel signals with 161.95 MHz center frequency are converted into 41.95 MHz digital IF signals. And the ASM 2 channel signals with 162 MHz center frequency are converted into 42 MHz digital IF signals. All the experiments in this paper are based on these digital IF signals and are carried out in the correlator of the IF circuit. The frequency of the master clock used in the experiments is 120 MHz.

3.2. Implementation of the Proposed Method. According to the correlation curve given in Figure 3(b), the linear relation between the correlation value and $\Delta\tau$ is affected by pulse shaping, while the symmetry of the correlation curve is not. In this case, the traditional maximum correlation value and E-L methods can cause a considerable error.

In this paper, the multicorrelator pseudorange measurement method was used and implemented as shown in Figure 5 to realize the proposed training sequence-based ranging method. It was implemented in the correlator design of the IF circuit based on the structure of the receiver shown in Figure 4. The influence of pulse shaping was also considered in this implementation, with the local reproduced baseband signal pulse shaped.

In the implementation diagram shown in Figure 5, the signal mapping module generates the I and Q branches of the 26-symbol double Barker code baseband signals. And then, the signals are pulse shaped by the root raised cosine filter with a roll-off coefficient of 0.35. Meanwhile, the local carrier generator generates the in-phase carrier signal $\cos \omega_c t$ and the quadrature carrier signal $-\sin \omega_c t$ with the same frequency as the transmitted signal. The I and Q branch local carrier signals and the I and Q branch local baseband signals are then multiplied by each other and added to get the I and Q branch local reproduced IF signal. Delay the local reproduced IF signals with the same time intervals t_d to get 1 + 2M duplicated signals. Finally, the received signal and the local signals are noncoherent correlated to get 1 + 2M correlation values.

The 1 + 2M correlation values can be centered with the maximum correlation value by adjusting the delay time of local reproduced IF signals. In addition to the maximum correlation value, there are M groups of correlation values. Each group includes two correlation values that are Ek and Lk. The Ek is $k \cdot t_d$ earlier than the centered maximum correlation value, and the Lk is $k \cdot t_d$ time later. After calculating the average of the earlier M correlation values $E_1, E_2, E_3 \cdots E_M$ and the later M correlation values $L_1, L_2, L_3 \cdots L_M$, respectively, the relation with $\Delta\tau$ is established:

$$\Delta\tau = c \cdot \frac{\sum_{i=1}^{M} E_i - \sum_{i=1}^{M} L_i}{\sum_{i=1}^{M} E_i + \sum_{i=1}^{M} L_i}. \tag{15}$$

$\Delta\tau$ can be used to calculate the value of TOA. Since the transmission time t_T is the beginning of the slot, the pseudorange measurement value can be calculated according to Section 2.2.2.

4. Results and Discussion

4.1. Correlation Results and Discussion. The correlation experiments were carried out to

(1) verify the advantage of using pulse shaping filter for local reproduced signal in the proposed receiver structure

(2) test the correlation property in different noise conditions

There were mainly three steps in the correlation experiments:

(1) Generated the received signal in different noise conditions

(2) Generated local reproduced signal

(3) Did the correlation operation to get the correlation curve

4.1.1. Received Signal. Since the distance between transmitter and receiver is limited in VDES, only the received signals in a limited range are needed for the correlation process. The received signal generated by simulation is a digital IF signal of 32-symbol sequence, which is comprised of 1-symbol

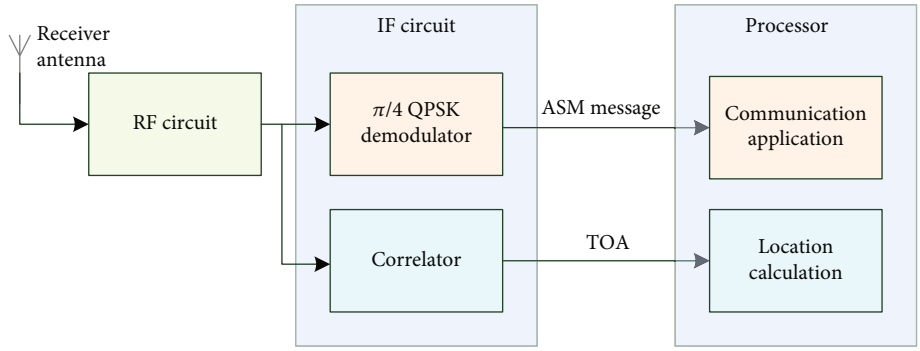

Figure 4: Block diagram of ASM channel receiver structure.

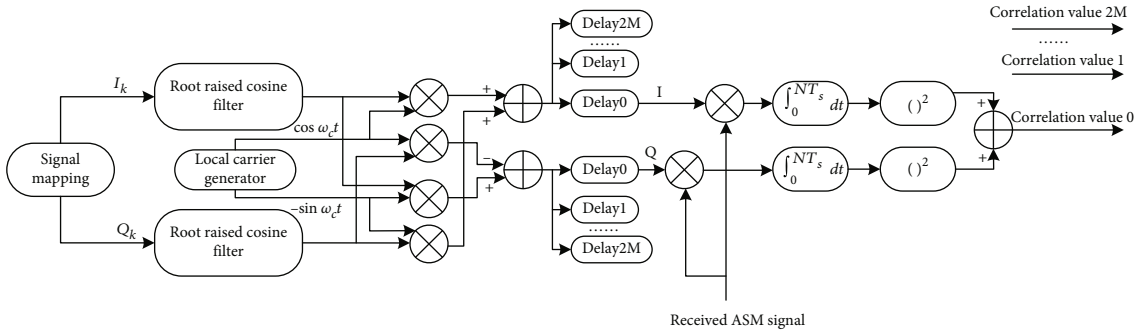

Figure 5: Implementation diagram of multicorrelator pseudorange measurement method.

ramp up (0), 27-symbol training sequence (1 1 1 1 1 1 0 0 1 1 0 1 0 1 0 0 0 0 0 1 1 0 0 1 0 1 0), and the following 4-symbol link ID (0 1 0 1). The frequency of the master clock used in the experiments is 120 MHz as introduced in Section 3.1, the symbol rate of ASM signal used in the experiments is 9600 sps, and then, 1/11 sampling is used to reduce the computation burden. Therefore, the data points of the generated received digital IF signal is as follows:

$$P_R = 32\text{symbols} \cdot \frac{1}{9600\ \text{sps}} \cdot 120\text{MHz} \cdot \frac{1}{11} = 3.6364 \times 10^4. \tag{16}$$

Besides, the received signal should be pulse shaped by root raised cosine filter with a roll-off coefficient of 0.35 in the transmitter and should be added some noise in the transmission channel.

Figure 6 shows the 36364 points of the received digital IF signal, which is pulse shaped in the transmitter and added some Additive White Gaussian Noise (AWGN) in the transmission channel. The Signal-to-Noise Ratio (SNR) decreases with the increase of noise, and it can be seen from Figure 6 that when the SNR is less than -20 dB, the changes in amplitude of the received digital IF signal which caused by the pulse shaping is hidden in the noise.

4.1.2. Local Reproduced Signal. The local reproduced signal generated by simulation is a digital IF signal of the 26-symbol sequence, which is the double Barker 13 code of the training sequence (1 1 1 1 1 0 0 1 1 0 1 0 1 0 0 0 0 0 1 1 0 0 1 0 1 0). The frequency of the master clock is 120 MHz, the symbol rate is 9600 sps, and 1/11 sampling is used. These parameters are exactly same as those in the generation of the received signal. The data points of the local digital IF signal is

$$P_L = 26\text{symbols} \cdot \frac{1}{9600\ \text{sps}} \cdot 120\text{MHz} \cdot \frac{1}{11} = 2.9545 \times 10^4. \tag{17}$$

In order to verify the advantage of using pulse shaping filter for local reproduced signal in the proposed receiver structure, the local reproduced signals with and without pulse shaping are both generated. Figure 7 shows the 29545 points of the local reproduced I and Q branch baseband signals with and without pulse shaping. It can be seen from the figure that the amplitude of the baseband signals changes continuously after the pulse shaping.

The baseband signals shown in Figure 7 are then modulated by the local generated carrier signal to get the local reproduced digital IF signals, which are needed in the correlation experiments.

4.1.3. Correlation Results and Discussion. Twenty experiments were carried out based on the received digital IF signals and the local reproduced digital IF signals. In each

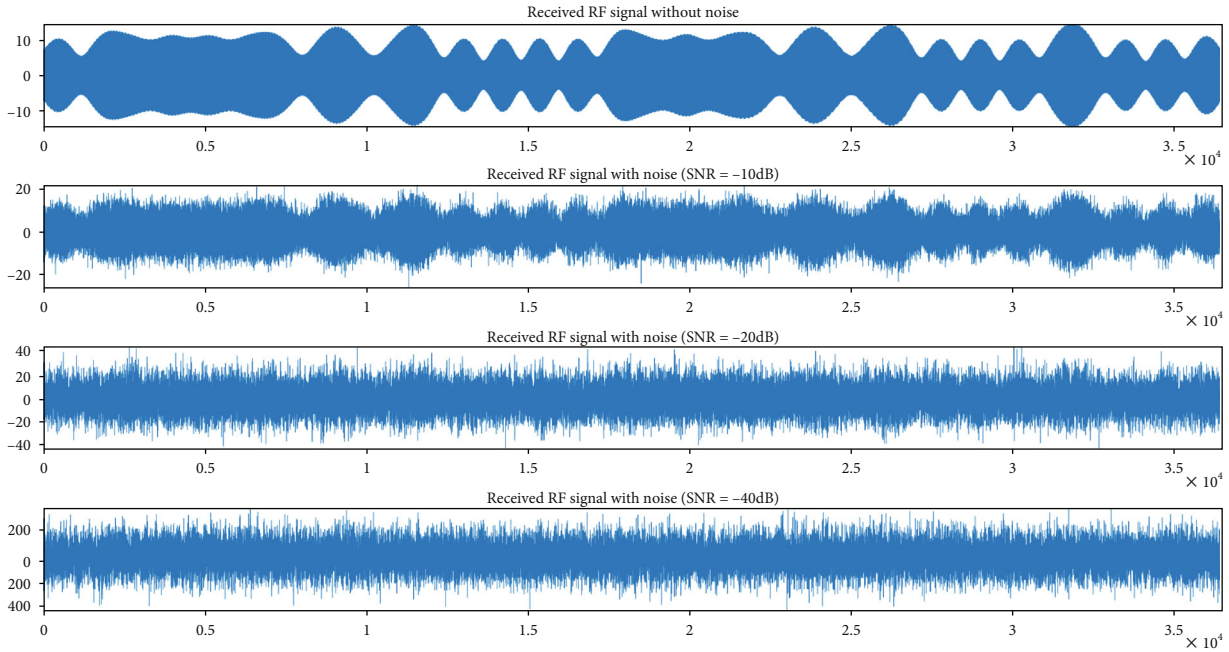

Figure 6: Received RF signal in different noise conditions.

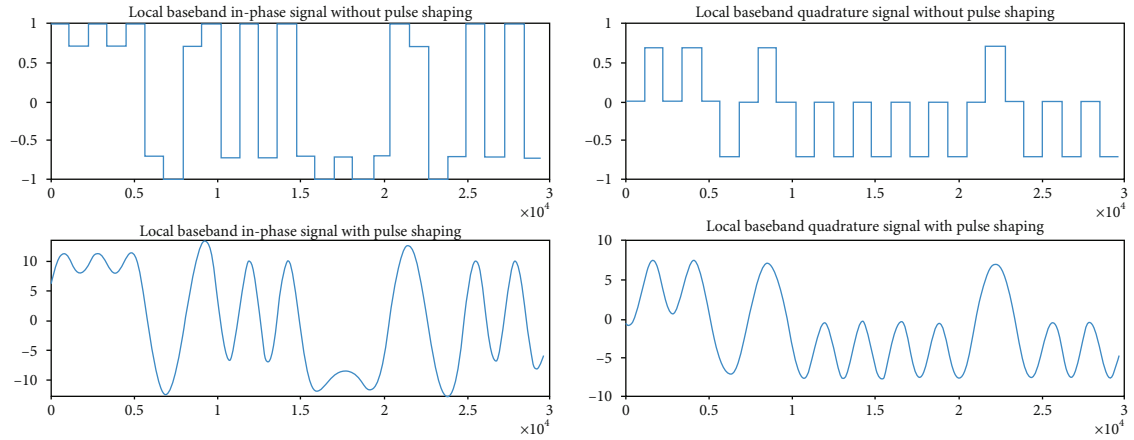

Figure 7: Local reproduced baseband of 26-symbol training sequence before and after pulse shaping.

experiment, the local reproduced digital IF signals with pulse shaping and without pulse shaping are, respectively, noncoherent correlated the same received signal to get two correlation curves at the same time. The shape of the correlation curves changed in each experiment, because the noise added to the received signal in the transmission channel was random.

Three typical experiment results are shown in Figure 8. It can be seen clearly that, if the local reproduced signals are pulse shaped, the correlation curves are obviously distorted when the SNR of the received signals are lower than -30 dB. While the local reproduced signals are not pulse shaped, the correlation curves are obviously distorted when the SNR of the received signals are lower than -20 dB. The results can verify the advantage of using pulse shaping filter for local reproduced signal in the proposed receiver structure. The results also can show the correlation property in different noise conditions.

4.2. Ranging Results and Discussion. Based on the receiver structure given in Section 3.1, the implementation of the multicorrelator pseudorange measurement method in Section 3.2 was used for the ranging experiments, where the number of the multicorrelators was $1 + 2M = 21$.

At the same time, the traditional maximum correlation value method and E-L method were also used for the ranging experiments to compare with the proposed multicorrelator method, in both conditions that the local reproduced

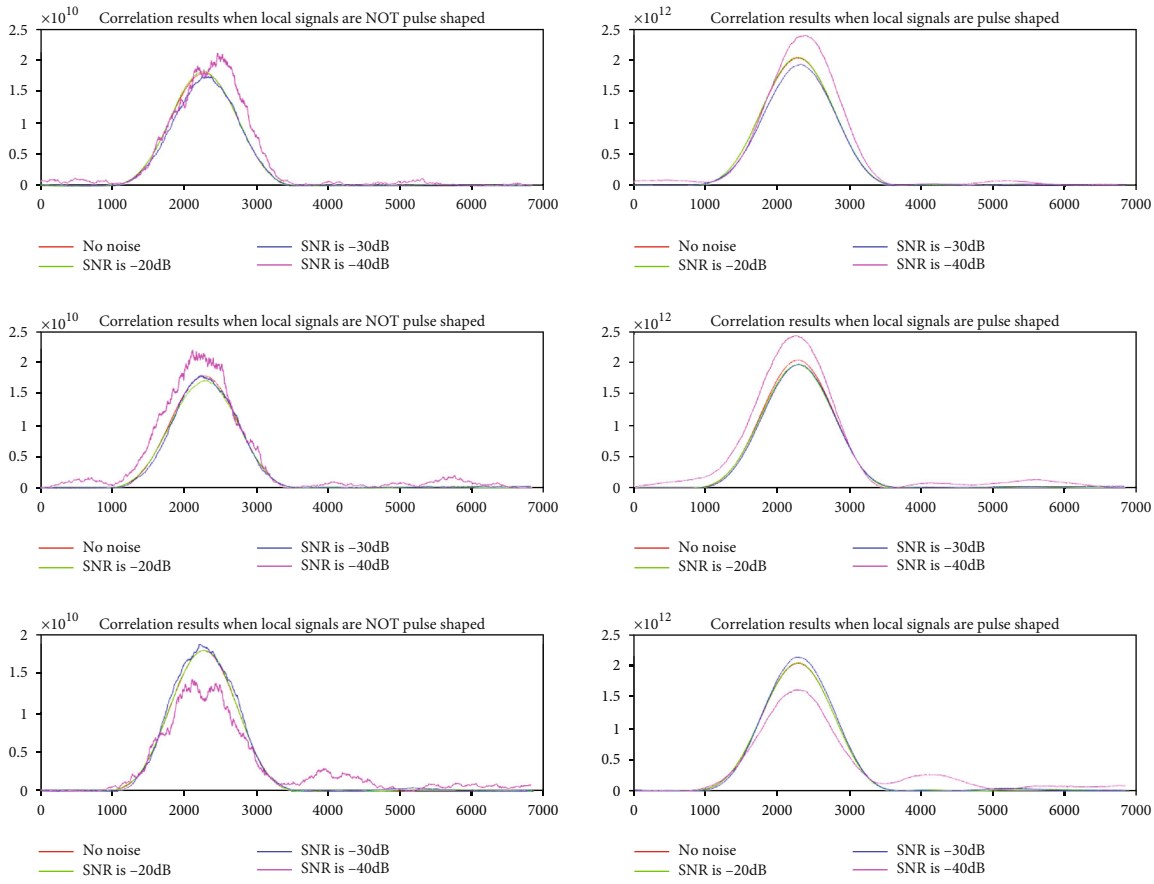

Figure 8: Correlation results of three experiments.

signal was pulse shaped and the local reproduced signal was not pulse shaped. The traditional maximum value method uses one or multiple correlators to get the correlation values in the phase range of [-1, +1] chips between the local reproduced signal and the received signal. The code phase of maximum correlation value is considered to be the synchronous phase. The traditional E-L method uses two correlators with fixed intervals. When the correlation values are equal in the phase range of [-1, +1] chips between the local reproduced signal and the received signal, the middle of the two correlators is considered to be the synchronous phase [53].

The results of ranging experiments using the three methods in the two conditions just described above are shown in Figure 9. It shows the TOA errors in different noise conditions. Figure 9(a) shows the experiment results in a big range of $-30\,\text{dB} < E_S/N_0 < 30\,\text{dB}$. In order to see clearly the experiment results in better noise condition, enlarged results in a smaller range of $-5\,\text{dB} < E_S/N_0 < 30\,\text{dB}$ are shown in Figure 9(b).

Figure 9(a) shows that when E_S/N_0 is less than -5 dB, the proposed multicorrelator method cannot get higher ranging accuracy compared with the other two methods, because the poor signal quality leads to serious distortion of correlation curve. Figure 9(a) also shows that the receiver can get higher ranging accuracy when local reproduced signal is pulse shaped.

Figure 9(b) shows when E_S/N_0 is greater than -5 dB, the proposed multicorrelator method can get higher ranging accuracy compared with the other two methods. And the performance is better when using pulse shaping filter for local reproduced signal. This is also the signal quality required by the communication function in VDES [44]. Figure 9(b) also shows that when E_S/N_0 is greater than 15 dB, the TOA error of the proposed method is less than 10 ns; that is, the accuracy of the pseudorange measurement value is better than 3 m.

According to the results, it can be concluded that when the signal quality is high, the proposed multicorrelator method can realize high accuracy ranging of the communication system. The ranging accuracy can be higher compared with the traditional maximum correlation value method and E-L method. Compared with the general VDES function, it does not occupy any additional time slot resources. This method can be used for VDES R-Mode receiver which generally works under good signal conditions. It can get the pseudorange value between the receiver and the base station. When getting more than three pseudorange values, the receiver can calculate its position. So the VDES R-Mode can be a backup land-based radio navigation system for GNSS, to reduce the impact of GNSS vulnerability, and contribute to the ship safety.

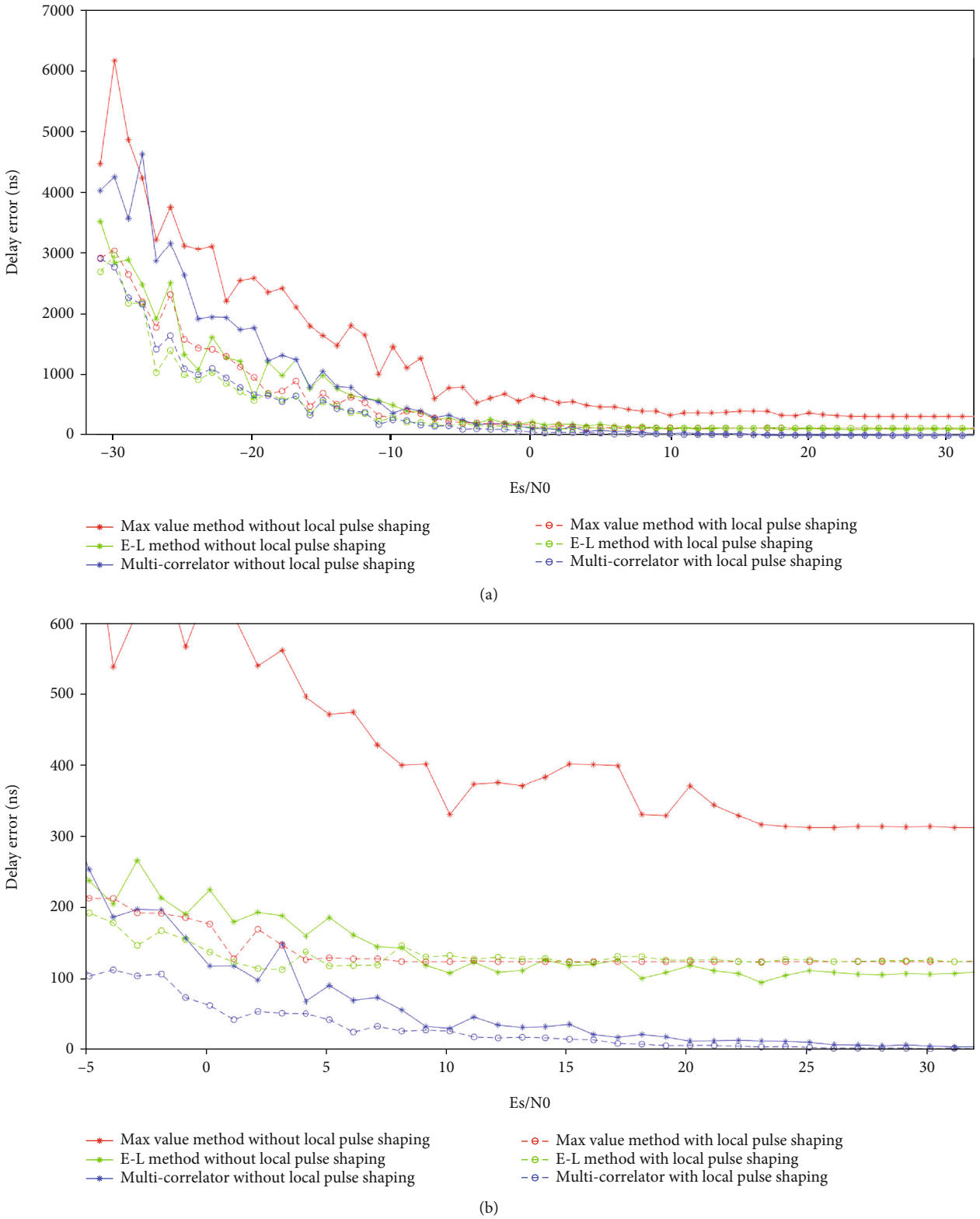

Figure 9: Experiment results of three methods: (a) TOA error when $-30\,\text{dB} < E_s/N_0 < 30\,\text{dB}$; (b) TOA error when $-5\,\text{dB} < E_s/N_0 < 30\,\text{dB}$.

5. Conclusions

This paper proposes a multicorrelator pseudorange measurement method based on the training sequence, which is normally used to capture and synchronize the communication signal. This method can be used for the R-Mode of the VDES. It uses the correlation property of the training sequence in ASM channel and VDE channel for ranging,

so it can realize ranging while communicating without occupying any additional time slot resources.

This paper also gives a receiver design based on the proposed method with a structure of multicorrelator after discussing the influence on the ranging performance of the pulse shaping required in the VDES. The baseband signal of the training sequence is reproduced in the receiver. It is then pulse shaped and becomes digital IF signal after carrier modulation. The IF signal noncoherent correlates with the received signal to get the correlation value which can be used to calculate the TOA, which can be used to get the pseudorange measurement value for positioning. The received signal is also a digital IF signal, which is the RF signal received by the antenna which goes through the downconverting and the A/D sampling in the RF circuit. To reduce the influence of the pulse shaping on the correlation curve, the pseudorange measurement method with multicorrelators is used to effectively reduce the pseudorange measurement error. The experiment results show that, compared with the traditional maximum correlation value method and E-L method, the multicorrelator pseudorange measurement method has higher ranging accuracy. When E_s/N_0 is greater than 15 dB, the ranging accuracy of the proposed method can be better than 3 m. The proposed multicorrelator pseudorange measurement method based on the training sequence can realize high accuracy ranging without occupying any additional time slot resources. It can provide a reference for the future research of the VDES R-Mode, which can be used to solve the vulnerability problem of the GNSS on maritime communication, so as to make a certain contribution to the robustness of 6G network space-time reference.

Data Availability

The data presented in this study are available on request from the corresponding author.

Conflicts of Interest

The authors declare no conflict of interest.

Authors' Contributions

S.X. and H.Q. were responsible for conceptualization. S.X. was responsible for the methodology, formal analysis, writing the original draft preparation, writing, review, and editing. J.Y. and S.X. were responsible for the software. S.X., H.Q., and J.Y. were responsible for the validation. H.Q. was responsible for the investigation, resources, supervision, and project administration. J.Y. was responsible for the data curation, visualization, and funding acquisition. All authors have read and agreed to the published version of the manuscript.

Acknowledgments

This research was funded by the National Program on Key R&D Project of China (2021YFB3901500) and the National Natural Science Foundation of China (52071047). This research was also supported by Joint Fund of the Natural Science Foundation of Liaoning Province of China (2020-HYLH-42) and the Fundamental Research Funds for the Central Universities (No. 017190327).

References

[1] Z. Na, Y. Liu, J. Shi, C. Liu, and Z. Gao, "UAV-supported clustered NOMA for 6G-enabled Internet of Things: trajectory planning and resource allocation," *IEEE Internet of Things Journal*, vol. 8, no. 20, pp. 15041–15048, 2021.

[2] Z. Na, B. Li, X. Liu et al., "UAV-based wide-area Internet of Things: an integrated deployment architecture," *IEEE Network*, vol. 35, no. 5, pp. 122–128, 2021.

[3] M. Zhou, Y. X. Lin, N. Zhao, Q. Jiang, X. L. Yang, and Z. S. Tian, "Indoor WLAN intelligent target intrusion sensing using ray-aided generative adversarial network," *IEEE Transactions on Emerging Topics in Computational Intelligence*, vol. 4, no. 1, pp. 61–73, 2020.

[4] IALA, *Recommendation R-129 GNSS Vulnerability and Mitigation Measures, Edition 3*, IALA, Saint Germain en Laye, France, 2012.

[5] P. Grant, N. Williams, S. Ward, and S. Basker, "GPS jamming and the impact on maritime navigation," *Journal of Navigation*, vol. 62, no. 2, pp. 173–187, 2009.

[6] IALA, *World Wide Radio Navigation Plan*, IALA, Saint Germain en Laye, France, 2nd ed edition, 2012.

[7] ITU, *Recommendation ITU-R M.1371-4 Technical Characteristics for an Automatic Identification System Using Time-division Multiple Access in the VHF Maritime Mobile Band*, ITU, Geneva, Switzerland, 2010.

[8] S. L. Eun, J. M. Amit, Y. M. Sang, and S. K. Geun, "The Maturity of automatic identification systems (AIS) and its implications for innovation," *Journal of Marine Science and Engineering*, vol. 7, no. 9, p. 287, 2019.

[9] ITU, *Automatic Identification System VHF Data Link Loading, Report ITU-R M.2287-0*, ITU, Geneva, Switzerland, 2013.

[10] J. Šafár, C. Hargreaves, and N. Ward, "The VHF data exchange system," in *Antennas, Propagation RF Technology for Transport and Autonomous Platforms*, Curran Associates, Inc., Red Hook, NY, USA, 2017.

[11] ITU, *Recommendation ITU-R M.2092-0 Technical Characteristics for a VHF Data Exchange System in the VHF Maritime Mobile Band*, ITU, Geneva, Switzerland, 2015.

[12] F. Clazzer, A. Munari, and F. Giorgi, "OCEANS 2017-Aberdeen," in *Asynchronous random access schemes for the VDES satellite uplink*, IEEE, Aberdeen, UK, 2017.

[13] J. Yi, Z. Yang, and W. Junsen, "A novel random access algorithm for very high frequency data exchange (VDE)," *Journal of Marine Science and Engineering*, vol. 8, no. 2, p. 83, 2020.

[14] K. M. Kim, Y. Kim, Y. Cho et al., "Performance evaluation of maritime VDES networks with OPNET simulator," in *2018 11th International Symposium on Communication Systems, Networks and Digital Signal Processing (CSNDSP)*, Budapest, Hungary, 2018.

[15] IMO, *Resolution MSC.401 (95) Performance Standards for Multi-System Shipborne Radionavigation Receivers*, IMO, London, UK, 2015.

[16] G. M. Huang, T. Jing, and W. Tian, "Survey on navigation via signal of opportunity," *Control and Decision*, vol. 34, no. 6, pp. 1121–1131, 2019.

[17] T. O. Mansfield, B. V. Ghita, and M. A. Ambroze, "Signals of opportunity geolocation methods for urban and indoor environments," *Annals of Telecommunications*, vol. 72, no. 3-4, pp. 145–155, 2017.

[18] G. G. Seco, S. J. López, and B. D. Jiménez, "Challenges in indoor global navigation satellite systems: unveiling its core features in signal processing," *IEEE Signal Processing Magazine*, vol. 29, no. 2, pp. 108–131, 2012.

[19] F. Coluccia, G. Ricciato, and G. Ricci, "Positioning based on signals of opportunity," *IEEE Communications Letters*, vol. 18, no. 2, pp. 356–359, 2014.

[20] S. Dammann and R. R. Sand, "Signals of opportunity in mobile radio positioning," in *2012 Proceedings of the 20th European Signal Processing Conference (EUSIPCO)*, pp. 549–553, Bucharest, Romania, 2012.

[21] V. Otsason, A. Varshavsky, and A. Lamarca, "Accurate GSM indoor localization," in *International conference on ubiquitous computing*, Springer Heidelberg, Berlin, 2005.

[22] M. Borenovic, A. Neskovic, and N. Neskovic, "Vehicle positioning using GSM and cascade-connected ANN structures," *IEEE Transactions on Intelligent Transportation Systems*, vol. 14, no. 1, pp. 34–46, 2013.

[23] M. A. Enright, H. Sridhara, and T. Nguyen, "Advanced GNSS integrity using signals of opportunity," in *Proceedings of the International Technical Meeting of the Institute of Navigation*, pp. 83–89, Newport Beach, CA, 2012.

[24] N. Yang and D. Q. Thao, "Positioning with mixed signals of opportunity," in *Institute of Navigation Satellite Division Proceedings of the International Technical Meeting*, pp. 447–456, Portland, OR, 2011.

[25] L. Chen, L. L. Yang, J. Yan, and R. Chen, "Joint wireless positioning and emitter identification in DVB-T single frequency networks," *IEEE Trans on Broadcasting*, vol. 63, no. 3, pp. 577–582, 2017.

[26] T. A. Webb, P. D. Groves, and P. A. Cross, "A new differential positioning method using modulation correlation of signals of opportunity," in *IEEE/ION Position, Location and Navigation Symposium*, pp. 972–981, New York, 2010.

[27] H. Simkovits, A. J. Weiss, and A. Amar, "Navigation by inertial device and signals of opportunity," *Signal Processing*, vol. 131, no. 2, pp. 280–287, 2017.

[28] J. J. Morales and Z. M. Kassas, "Distributed signals of opportunity aided inertial navigation with intermittent communication," in *Institute of Navigation Satellite Division Proceedings of the International Technical Meeting*, pp. 2519–2530, Portland, Oregon, 2017.

[29] K. M. Pesyna, K. D. Wesson, and R. W. Heath, "Extending the reach of GPS-assisted femtocell synchronization and localization through tightly-coupled opportunistic navigation," in *IEEE Globecom Workshops*, pp. 242–247, Houston, 2011.

[30] G. W. Johnson and P. F. Swaszek, "Feasibility study of R-mode using MF DGPS transmissions," *German Federal Waterways and Shipping Administration, Milestone 2 Report*, IALA, Saint Germain en Laye, France, 2014.

[31] G. W. Johnson and P. F. Swaszek, "Feasibility study of R-mode using AIS transmissions," *German Federal Waterways and Shipping Administration, Milestone 4 Report*, IALA, Saint Germain en Laye, France, 2014.

[32] G. W. Johnson and P. F. Swaszek, "The feasibility of R-mode to meet resilient PNT requirements for e-navigation," in *Proceedings of the 27th International Technical Meeting of The Satellite Division of the Institute of Navigation (ION GNSS+2014)*, pp. 3076–3100, Tampa, Florida, 2014.

[33] J. Šafár, A. Grant, P. Williams, and N. Ward, "Performance bounds for VDES R-mode," *The Journal of Navigation*, vol. 73, no. 1, pp. 92–114, 2020.

[34] Q. Hu, Y. Jiang, J. Zhang, X. Sun, and S. Zhang, "Development of an automatic identification system autonomous positioning system," *Sensors*, vol. 15, no. 11, pp. 28574–28591, 2015.

[35] Y. Jiang, J. Wu, and S. Zhang, "An improved positioning method for two base stations in AIS," *Sensors*, vol. 18, no. 4, 2018.

[36] H. Qing, J. Xiaoyue, and L. Pengfei, "A novel carrier frequency offset algorithm based on a double Barker code in VDE-TER," *Physical Communication*, vol. 40, p. 101059, 2020.

[37] S. Gewies, A. Dammann, R. Ziebold et al., "R-Mode testbed in the Baltic Sea," in *Proceedings of the 19th IALA Conference*, Incheon, Korea, 2018.

[38] M. Hoppe, A. Grant, C. Hargreaves, and P. Williams, "R-Mode: the story so far,," in *Proceedings of the 19th IALA Conference*, Incheon, Korea, 2018.

[39] K. Paul and G. Stefan, "Worldwide availability of maritime medium-frequency radio infrastructure for R-Mode-supported navigation," *Journal of Marine Science and Engineering*, vol. 8, no. 3, p. 209, 2020.

[40] J. Zhang, S. Zhang, and J. Wang, "Pseudorange measurement method based on AIS signals," *Sensors*, vol. 17, no. 5, p. 1183, 2017.

[41] M. Wirsing, A. Dammann, and R. Raulefs, "Investigating R-Mode signals for the VDE system," in *OCEANS 2019 MTS/IEEE SEATTLE*, pp. 1–5, Seattle, WA, USA, 2019.

[42] IALA, *Guideline G1139-The Technical Specification of VDES, Edition 3*, 2019.

[43] F. Lázaro, R. Raulefs, H. Bartz, and T. Jerkovits, "VDES R-Mode: vulnerability analysis and mitigation concepts," *International Journal of Satellite Communications and Networking*, 2021.

[44] J. Šafář, A. Grant, and M. Bransby, "Performance bounds for VDE-SAT R-mode," *International Journal of Satellite Communication Network*, 2021.

[45] X. M. She and D. Weiwei, "Viterbi detection method of $\pi/4$-QPSK signal in VDE," *Procedia Computer Science*, vol. 107, pp. 539–544, 2017.

[46] D. Divsalar and M. K. Simon, "Multiple-symbol differential detection of MPSK," *IEEE Transactions on Communications*, vol. 38, no. 3, pp. 300–308, 1990.

[47] S. R. Theodore and Q. M. Meng, *Wireless Communications Principles and Practice*, Publisher: Publishing House of Electronics Industry Beijing, China, 2nd ed edition, 2018.

[48] C. Sandeep and G. J. Saulnier, "Differential detection of pi /4-shifted-DQPSK for digital cellular radio," *IEEE Transactions on Vehicular Technology*, vol. 42, no. 1, pp. 46–57, 1993.

[49] P. Jiang and X. Hou, "$\Pi/4$-DQPSK demodulation based on DSTFT," *Journal of Telemetry, Tracking and Command*, vol. 28, no. 1, pp. 1–4, 2007.

[50] M. Y. Zhang and Y. Z. Zhang, "An integrated demodulation technology of variable signal of $\pi/4$-DQPSK and GMSK modulation," *Journal of Radio Engineering*, vol. 45, no. 2, pp. 30–33, 2015.

[51] Y. T. Ma, K. Pahlavan, and Y. S. Geng, "Comparison of POA and TOA based ranging behavior for RFID application," in *Proceedings of the 2014 IEEE 25th Annual International Symposium on Personal, Indoor, and Mobile Radio Communication*, pp. 1722–1726, Washington, DC, USA, 2014.

[52] H. Nyquist, "Certain topics in telegraph transmission theory," *Transactions of the AIEE*, vol. 47, no. 2, pp. 617–644, 1928.

[53] D. Kaplan, *Understanding GPS: Principles and Applications, Second Edition, Norwood*, Artech House, MA, 2006.